22nd Iranian Conference on Biomedical Engineering(ICBME 2015), Iranian Research Organization for Science and Technology (IROST), Tehran, Iran, 25-27 November 2015

Improving Active Shape Models Performance in Low-Contrast Images Using a KNN-based Search Algorithm

With Applications In Liver Segmentation

Mina Esfandiarkhani*, Mahdi Delavari,
Amir Hossein Foruzan
Department of Biomedical Engineering, Shahed University, Tehran, Iran.
m.ekhani@shahed.ac.ir, md.delavari@shahed.ac.ir, a.foruzan@shahed.ac.ir

Yen-Wei Chen
Intelligent Image Processing Lab, College of Information Science and Engineering, Ritsumeikan University, Japan.
chen@ritsumei.ac.jp

Abstract— **Active Shape Model (ASM) is considered as a high level image processing algorithm. Typical applications include image segmentation and interpretation. A major challenge in ASMs is to repeatedly move model points towards true boundaries. It is a crucial step in the algorithm which fails in cases of low contrast images. In this paper, we present a new search algorithm for ASM to tackle segmentation of tissues with nearby organs of similar intensities. We train a KNN classifier and employ it to label the region surroundings each mesh point and move the point towards the boundary. Thus, evolution of the initial surface is performed faster in a single step. Evaluation of the proposed method was carried out by Dice and Jaccard similarity measure and accuracy index. The results of segmentation were compared with the results of Active Contour Model and conventional ASM. The Dice (Jaccard) indices are 0.93 (0.87), 0.85 (0.73) and 0.9 (0.76) for our method, conventional ASM and ACM, respectively. Moreover, the accuracy is increased in the proposed method compared to the two other methods.**

Keywords: Active Shape Models, Search Algorithm, KNN Classification, Liver Segmentation.

I. INTRODUCTION

The conventional Active Shape Model (ASM) proposed by Cootes et al. [1] uses a statistical model of shape extracted from landmarks and gray level profiles along the normal direction at each point. Mean shape is computed from aligned shapes and main variations of modes are achieved by applying Principle Component Analysis on the covariance matrix of landmark coordinates. A shape model is constructed by linear combination of the mean shape and a few first modes. When the model is employed in segmentation of a new image, relocating of the initial mesh points is performed by comparing the current gray level profile in each point with the mean normal profile. A point is moved so that the distance between the two profiles is minimized using a cost function [2]. Applications of ASM include image segmentation, organs volume estimation such as prostate [3], diagnose and treatment of skeletal disease [4], extraction of lip contours to improve visual speech [5], shape variations analysis and reconstruction.

Image segmentation is used in different fields such as machine vision, object detection and especially in medical imaging. Medical image segmentation is employed to locate tumors, measure tissue volumes, identify anatomical structure and surgery planning. There are several algorithms to implement segmentation but in recent two decades model-based algorithms have been implemented as a successful method in image representation. Because of applying some constraints to the shape, ASM provides reliable results compared to other algorithms [2]. Major challenges in implementing an ASM include: (1) Finding correspondence between points in training samples which greatly affects statistical shape model. (2) Requiring a large number of training images to cover shape variations [6]. (3) Using an efficient and effective search algorithm to place mesh points in the appropriate position to accurately define the boundary of an object. In our previous work, we proposed a fast non-rigid algorithm to find corresponding points which improved the performance of the ASM compared to "Iterative Closest Point" (ICP) and "Thin Plate Spline-Robust Point Matching: (TPS-RPM) methods [6]. In this paper, we address the third challenge using a new fast search algorithm.

II. PREVIOUS WORKS

As mentioned in section I, the search algorithm is considered as a crucial step in the ASM segmentation pipeline. Except for the Cootes' algorithm which explicitly employs the normal profile of mesh points, most of the ASM-based segmentation methods adopt a feature-based approach in their search algorithm. In medical images, however, the profiles of boundary points do not follow a gaussain distribution. Therefore, the Mahalanobis distance is not a proper cost function for optimal displacement of mesh points and non-

978-1-4673-9351-5/15/$31.00 ©2015 IEEE

linear methods are more popular. Training a classifier with features extracted in landmark points and reconstructing a shape with new positions is the preferred approach to enhance the search algorithm. Some researches proposed an iterative approach to put the mesh points on the boundary of the object which requires a lot of time and a large amount of memory.

Ginneken *et al.* [7] computed moments of the local histogram of mesh points via Gaussian derivatives filter bank and employed KNN classifier to achieve displacements of landmarks. Toth et al. [3] presented Multi-Feature ASM. Forward feature selection was used to get discriminatory textural properties and to generate the appearance model. They extracted boundary features with conventioanl filters including Sobel, Gaussian and Mean. Ebhotemhen [8] segmented the lateral ventricle of brain by a hybrid KNN-ASM method. He extracted local edge features via Haar filters and then trained a KNN classifier to place landmark points in their best positions. Li et al. [9] used AdaBoost algorithm and trained it with features calculated by steerable filters. Bailleul et al. [9] got features along the normal of landmark point including maximum intensity difference between inside and outside voxels and intensity means difference.

In this paper, we present an innovative approach for the search algorithm which better can estimate the true position of landmarks on the border of an object. We use KNN classifier and morphological filters to find the boundary of the object near each landmark and to relocate the point from its initial position to the final location. The movement is carried out in a single step which increases the speed of the code. The KNN is trained locally using the features of each landmark. We employed our method to segment liver in Computed Tomography images. Segmentation results are improved compared to the traditional algorithm, where an image has low contrast and the gland is in contact with tissues of the same intensity range. Regarding Dice and Jaccard measures, our results are superior to the conventional ASM and Active Contour methods.

Kass et al. introduced active contours (snake) as flexible models to segment images and detect/track objects. Snakes are considered as parameterized models and their parameters are the position of boundary points. The corresponding energy function contains stiffness and elasticity terms as internal forces and a gradient-based term as the external force. The boundary points are moved toward salient image features such as lines and edges by image forces [1]. This method has inherent limitations. It needs a prior knowledge about the shape to be segmented and the results are sensitive to initialization and local gradients. Moreover, the boundary leaks to nearby organs in cases of low contrast images [7].

III. PROPOSED METHOD

The pipeline of our method is shown in Fig. 1. It consists of three main steps: (1) Building the liver active shape model (statistical shape model + gray level appearance model). (2) Training local KNNs. (3) Initial segmentation of an input image and refinement of the result by the proposed search method. To build an ASM, it is needed to represent input training shapes by a set of landmarks. Then, local intensity models of each landmark are prepared which is later employed to relocate a new shape points. At the location of a landmark, a KNN is considered which is trained by the local features. Initialization of the model for an input image is performed by conventional segmentation methods including the Graphcut algorithm [10]. Then, the result is improved by our new search algorithm. Finally, segmented object's shape is refined by restricting the shape to valid ranges of the models parameters.

A. *Building Statistical Shape Model*

First, liver is segmented by our method described in [11]. Then, its surface is triangulated by the Marching Cube algorithm [12].

Initially, the number of points that describe liver surface is too much so we smooth and decimate landmarks to 1000 points.

Then, we build a Statistical Shape Model (SSM) of the input shapes. Each shape in training set is described by j landmark points as described in (1).

$$\begin{pmatrix} x_1 & y_1 & z_1 \\ \vdots & \vdots & \vdots \\ x_j & y_j & z_j \end{pmatrix} \rightarrow X = (x_1, y_1, z_1, ..., x_j, y_j, z_j)^T \quad (1)$$

Since liver is a non-rigid object, selecting a suitable non-rigid transformation to generate statistical shape model is very important [6]. Coherent Point Drift (CPD) algorithm is employed to find corresponding points of training set [13]. The next step is compute mean shape using generalized Procrustes analysis [14]. In this algorithm, one of the shapes in training set is considered as the reference and other shapes are aligned with

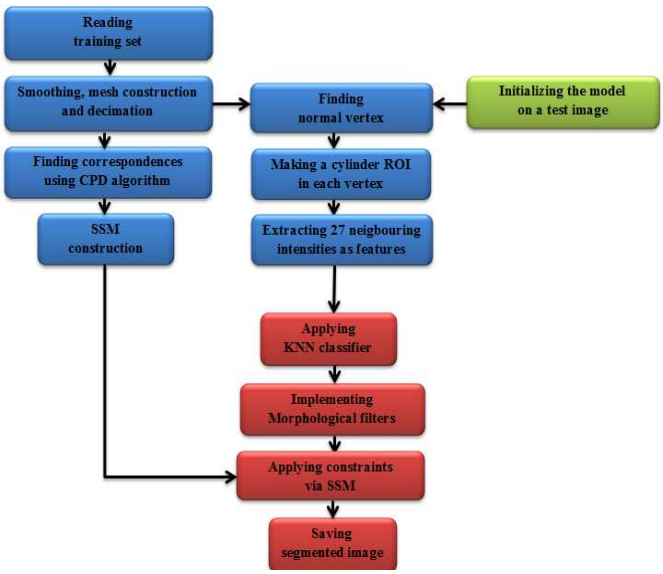

Figure 1. The flowchart of proposed method.

it. New mean shape is recalculated using (2) and this process is repeated until convergence. In (2), N is the number of shapes in training set. Next, the Covariance matrix is computed using (3).

$$\overline{X} = \frac{1}{N}\sum_{i=1}^{N} X_i \tag{2}$$

$$C_x = \frac{1}{N}\sum_{i=1}^{N}(X_i - \overline{X})(X_i - \overline{X})^T \tag{3}$$

The eigenvectors corresponding to the t largest eigenvalues are employed to reconstruct new valid shapes (4) and (5).

$$P = [P_0, P_1, \ldots, P_{2n-1}] \tag{4}$$

$$X = \overline{X} + Pb \tag{5}$$

In (5), 'b' is a vector containing the model parameters. Because 'P' is an orthogonal matrix so " $P^T = P^{-1}$ " and the model parameter is given by (6).

$$b = P^{-1}(X - \overline{X}) \tag{6}$$

A new shape vector (b) should be constrained in the range of $\pm\sqrt{3\lambda_i}$ to guarantee its validity.

The maximum number of the modes (t) is selected so that inequality (7) holds.

$$\sum_{i=1}^{t}\lambda_i \geq f_v \sum_{i=1}^{2n}\lambda_i \tag{7}$$

In (7), " f_v " is a certain proportion usually set to 0.98 [9] and the remaining $2n-t$ modes are considered as a shape noise [15].

B. Gray level appearance model

The gray level appearance is obtained by sampling along the positive and negative normal direction (k pixel either side) in each landmark point [16]. It is employed to link shape and intensity variations. The normal vector to a vertex in a mesh is calculated using the 'Mean Weighted by Angle (MWA) algorithm described by (8) [17].

$$N_{MWA} = \sum_{i=1}^{n}\alpha_i N_i \tag{8}$$

It is a weighted sum of normal vectors of neighboring surfaces. A neighboring surfaces contains a triangle including two edge vectors E_i and E_{i+1} . Alpha (α) is the angle between the two edges and is the computed by (9).

$$\sin\alpha = \frac{|E_i \times E_{i+1}|}{|E_i||E_{i+1}|} \tag{9}$$

Typical normal vectors overlaid on a mesh are shown in Fig. 2. The normalized profile is used to compute the mean profile vector and its modes so as to build the appearance model [18] (10) to (12).

$$g_{ij} = \begin{bmatrix} g_{ij0} & g_{ij1} & \cdots & g_{ijn_p-1} \end{bmatrix}^T \tag{10}$$

$$dg_{ij} = \begin{bmatrix} g_{ij1} - g_{ij0} & g_{ij2} - g_{ij1} & \cdots & g_{ijn_p-1} - g_{ijn_p-2} \end{bmatrix}^T \tag{11}$$

$$y_{ij} = \frac{dg_{ij}}{\sum_{k=0}^{n_p-2}|dg_{ijk}|} \tag{12}$$

In (10), g_{ij} is the gray level of the j^{th} landmark point in i^{th} shape and n_p is the length of the profile. Also dg_{ij} and y_{ij} are the derivative and normalized profiles, respectively.

Mean and covariance of the profiles of mesh points are given by (13) and (14).

$$\overline{y}_j = \frac{1}{N}\sum_{i=1}^{N} dg_{ij} \tag{13}$$

$$C_{yj} = \frac{1}{N}\sum_{i=1}^{N}(y_{ij} - \overline{y}_j)(y_{ij} - \overline{y}_j)^T \tag{14}$$

C. Conventional Search algorithm

To segment a new image, the shape model is initialized on the test image. Then, gray level profiles are generated according to (15) to (17).

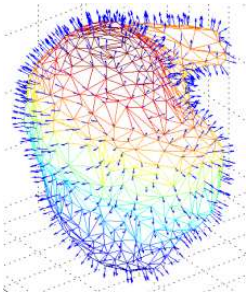

Figure 2. Typical normal vectors overlaid on a mesh.

$$s_j = \begin{bmatrix} s_{j0} & s_{j1} & \dots & s_{j,n_s-1} & s_{j,n_s-2} \end{bmatrix}^T \quad (15)$$

$$ds_j = \begin{bmatrix} s_{j1}-s_{j0} & s_{j2}-s_{j1} & \dots & s_{j,n_s-1}-s_{j,n_s-2} \end{bmatrix}^T \quad (16)$$

$$y_{sj} = \frac{ds_j}{\sum_{k=0}^{n_s-2} |ds_{jk}|} \quad (17)$$

Where s_j and n_s are the profiles along landmark points and the length of the profile, respectively. The length of the test profile should be larger than train profile $(n_s > n_p)$.

The search algorithm is based on the Mahalanobis distance. The distance should be iteratively minimized to achieve the best movement of landmarks. The cost function $f(d)$ is defined by Equation (18) [18].

$$f(d) = (h(d) - \bar{y}_j)^T C_{yj}^{-1} (h(d) - \bar{y}_j) \quad (18)$$

Exhaustive search is performed for each sub-interval of y_{sj} centered at d^{th} pixel and the similarity of the new profile to the mean profile is calculated. The corresponding mesh point is moved to the center of the profile where the cost function is minimized. This exhaustive search is done for all landmark points. The resulting shape is represented by the SSM model and shape parameters are constrained by (6) to insure similarity of the result to the training shapes.

The above approach is appropriate when the distribution of intensities is Gaussian which is always not the case. In the next subsection, we describe our proposed search algorithm which is non-iterative and cope with the problem of low contrast images.

D. The KNN-Based Search Algorithm

Our proposed KNN-Based search algorithm puts a landmark on the border of an object using a local supervised classifier which is trained by the intensities of nearby tissues. First, we assign a KNN classifier to each landmark, called local KNN, using sample intensities around the mesh point. A cylinder perpendicular to contour mesh is selected to train a local KNN. The cylinder is defined using the normal vector corresponding to the mesh point ((19) to (20)).

$$\left\langle (M_j - m_j), N \right\rangle \le L \quad (19)$$

$$(M_j - m_j) - N \le R \quad (20)$$

In (19) and (20), $(M_j - m_j)$ is the distance between mesh point and a nearby point. N, L, R are the axis (normal vector), length and radius of cylinder, respectively. The intensity of a 3x3x3 region around each point is selected as the feature vector of that point which is a vector of the size 1x27. Regarding the test image, intensity samples are achieved in the same way as the training step. After applying KNN, the region around a landmark is classified into object and background. We employ morphological filters to refine the results and remove false positives. We remove all connected components with fewer than 8 pixels from a binary image and the largest connected component is selected as the background. Then, a mesh point is put on the nearest location of the object's border (21).

$$m_j = argmin_j \left\| M_j - m'_j \right\|^2 \quad (21)$$

In (21), m'_j is a background point, M_j is the j^{th} landmark, and m_j is the new position of the landmark.

The new positions of all landmarks are found and the new shape is modified by the shape model by the following algorithm:

a) Initialize 'b' to zero.

b) Generate model with (5).

c) If the new positions are considered as 'Y', apply procrustes analysis to project model into Y in order to find pose parameters: translation (t), rotation (θ)and scale (S).

d) Apply inverse of pose parameters to 'Y' in the form of (22).

$$y = T_{(\theta,S,t)}^{-1}(Y) \quad (22)$$

e) Map the result into the tangant plane by (23).

$$y = y / (y.\bar{X}) \quad (23)$$

f) Update 'b' from (24).

$$b = P^{-1}(y - \bar{X}) \quad (24)$$

g) Constrain 'b', repeat from step "b" to "f" until convergence.

IV.RESULTS

A. Dataset

In this paper, 3D CT images of 10 abnormal livers in second phase from 6 males and 4 females in the range of 20 to 75 years old were used. The size of images and voxels were 512 x 512 x 159 and 0.63 x 0.63 x 1.25 mm^3 respectively. The dataset belong to Osaka University, Japan.

We implemented our method in MATLAB environment and ran in a personal computer with AMD-Radeon(TM) HD 6630M, 2.3GHz CPU and 6GB dynamic RAM, running Windows 7.

As previously mentioned, the surface of each liver is generated via Marching Cube Algorithm and the points are decimated to 1000 using MATLAB libraries. Visualization of the meshes is performed by 3D-Slicer [19]. To compare segmentation results with the manual segmentation, the meshes convert to binary image using VTK toolkit [20].

B. *Evaluation metrics*

We evaluated our method using Dice similarity coefficient, Jaccard, and accuracy. The Dice similarity measure is defined by (25).

$$S_{Dice} = \frac{2|M_{Auto} \cap M_{Gold}|}{|M_{Auto}| + |M_{Gold}|} \tag{25}$$

Where M_{Auto} and M_{Gold} are the volume segmented by our method and gold standard, respectively. In Fig. 3, Dice similarity measure of the segmentation of three test images with the proposed method and two other methods are shown. Surface visualization of ACM results are compared with the results of our method and also with the manually segmentation results in Fig.4.

Fig. 5 indicates the results of the Jaccard index for each test images. The Jaccard index is used for comparing the similarity and diversity of sample sets, introduced by (26).

$$S_{Jaccard} = \frac{|M_{Auto} \cap M_{Gold}|}{|M_{Auto} \cup M_{Gold}|} \tag{26}$$

In Table I, the accuracy in ACM and proposed method for three test images are shown and achieved by (27).

$$Accuracy = \frac{TP + TN}{TP + TN + FP + FN} \tag{27}$$

I. DISCUSSION

We introduced a new method for search algorithm in ASM. This method can relocate surface points to the true boundary of an object when the distribution of intensity profiles is not Gaussian. The average Dice (Jaccard) indices are 0.93 (0.87), 0.85 (0.73) and 0.9 (0.76) for our method, conventional ASM and ACM, respectively.

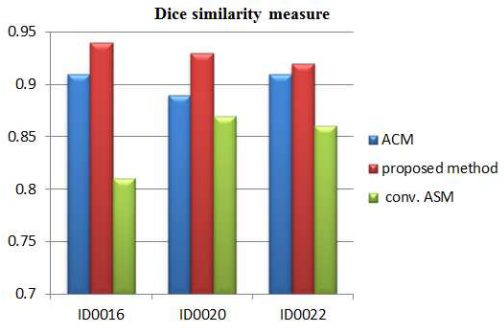

Figure 3. Typical Dice similarity measures for different test image.

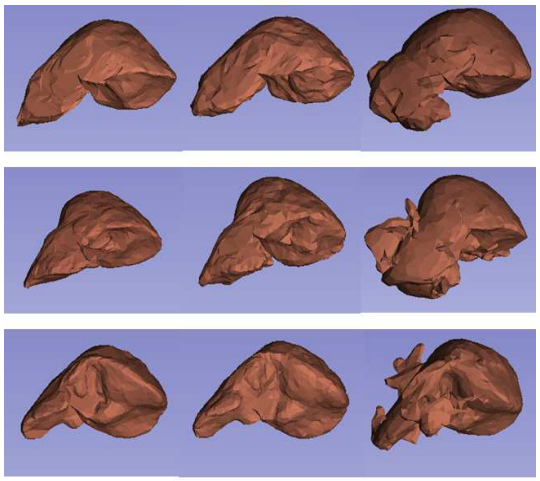

Figure 4. Typical visualization of the surface of liver. Column (a), (b) and (c) are segmentation with manual, proposed method and ACM . Rows are related to each test image.

TABLE I. COMPARISON OF ACCURACY OF THREE METHODS.

Accuracy	Method		
	ACM	*Proposed Method*	*Conv. ASM*
ID0016	0.98	0.99	0.98
ID0020	0.97	0.98	0.97
ID0022	0.98	0.99	0.97

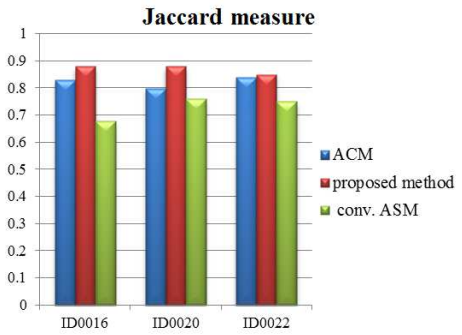

Figure 5. Typical Jaccard measures for three test images.

It is shown that our method outperforms conventional ASM and ACM algorithms. As can be seen in Fig. 6 intensities of colon, kidney, intercostal muscles and liver are similar. However, classification by local KNNs did not leak to nearby organs. Our method is faster than conventional ASM, the comparison of time in three method shows in TABLE II. After initialization of the mean shape, the final segmentation is obtained in a single step while in case of the conventional ASM an iterative approach achieves the results. Inclusion of morphological filters to remove false positive and selection of the largest connected component improved accuracy of our method too. Another achievement of our method is implementing local instead of global KNNs. Because the

intensities are different in each part of the liver, when we train and search locally in each region, the final results will be more reliable. Fig. 7 shows segmented boundary by (a) KNN-based and (b) conventional ASM. While conventional ASM achieved the results in 5 iterations, our approach reached the boundary in a single step.

VI. conclusion and future works

In this paper, we proposed a new approach to search algorithm in ASM segmentation. Our method is faster than conventional ASM and outperforms ASM and ACM algorithms regarding Dice and Jaccard metrics. In future we are going to improve the segmentation results by incorporating a confidence weight to mesh point movements, therefore, proposing a robust solution to segmentation of low-contrast images.

TABLE II. COMPARISON OF THE AVERAGE TIME IN THREE METHODS.

Average Time (s)	Method		
	ACM	*Proposed Method*	*Conv. ASM*
	80	190	340

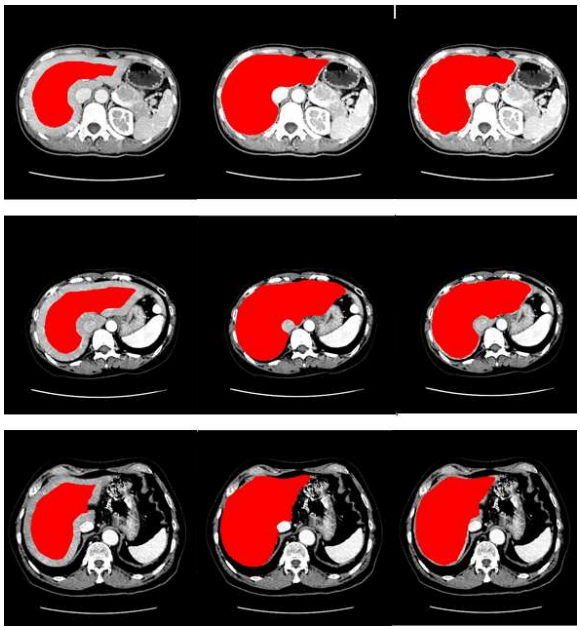

Figure 6. Liver segmentation in 106^{th} slice. Columns from left to right are initial, manual and proposed method, respectively. Rows are test images.

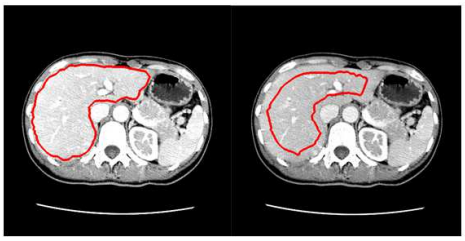

(a) (b)

Figure 7. Liver boundary acquired by (a) the proposed method, (b) conventional ASM in 5^{th} itteration.

References

[1] T.F.Cootes , C.J. Taylor, D.H. Cooper, and J. Graham, "Active shape models – their training and application," Computer Vision and Image Understanding, 61(1), pp. 38–59, Jan. 1995.

[2] T.F.Cootes, and C.J.Taylor, "Statistical Models of Appearance for Computer Vision," Wolfson Image Analysis Unit , Image Science and Biomedical Engineering ,University of Manchester,2001.

[3] R. Toth. et al. "Accurate Prostate Volume Estimation Using Multifeature Active Shape Models on T2-weighted MRI," Acad Radiol 2011; 18:745–754.

[4] N. Sarkalkan , H. Weinans, and A. A. Zadpoor, "Statistical shape and appearance models of bones," Bone 60 (2014) 129–140.

[5] S.L.Wang , W.H.Lau ,and S.H.Leung, "Automatic lip contour extraction from color images," Pattern Recognition 37 (2004) 2375 – 2387.

[6] M. Delavari, A.H. Foruzan, and Y. Chen. "Improvement of Statistical Shape Models for Soft Tissues Using Modified-Coherent Point Drift," 21st Iranian Conference on Biomedical Engineering(ICBME 2014),Tehran, Iran,Nov 26-28,2014.

[7] B. van Ginneken. et al. "Active Shape Model Segmentation With Optimal Feature," IEEE TRANSACTIONS on Medical Imaging, Vol. 21, No. 8, August 2002.

[8] E. Ebhotemhen, "Medical Image Segmentation using an Extended Active Shape Model," International Journal of Computer Applications (0975 – 8887) Volume 69– No.19, May 2013.

[9] T. Heimann, and H.p. Meinzer, "Statistical shape models for 3D medical image segmentation: A review," Medical image analysis, Vol. 13, No. 4, pp.543-563, May 2009.

[10] Y. Boykov, and M. P. Jolly, "Interactive organ segmentation using graph cuts," In Medical Image Computing and Computer-Assisted Intervention-MICCAI 2000 (pp. 276-286). Springer Berlin Heidelberg, 2000.

[11] A.H. Foruzan. et al. "Segmentation of Liver in Low-Contrast Images Using K-Means Clustering and Geodesic Active Contour Algorithms," IEICE TRANSACTIONS on Information and Systems, 2013; E96-D (4): 798-807.

[12] W.E. Lorensen, H.E Cline, Marching Cubes, "A high resolution 3D surface construction algorithm," Computer Graphics, 1987; 21(4): 163-169.

[13] A. Myronenko, and X. Song, "Point Set Registration: Coherent Point Drift," TPAMI, 2010; 32(12): 2262–2275

[14] J.C. Gower, "Generalized procrustes analysis," Psychometrika, Vol. 40, No. 1, pp. 33-51, Mar. 1975.

[15] M. B.Stegmann, Project Supervisor: R. Fisker, " On Properties of Active Shape Models," Department of Mathematical Modelling Technical University of Denmark DTU Building 321, DK-2800 Lyngby, Denmark, March 2nd 2000.

[16] M. Spiegel, Dieter A. Hahnb, Volker Daum, JakobWasza,and Joachim Hornegger, "Segmentation of kidneys using a new active shape model generation technique based on non-rigid image registration," Computerized Medical Imaging and Graphics 33 (2009) 29–39.

[17] Sh. Jin, R. Lewis,and D. West, "A Comparison of Algorithms for Vertex Normal Computation," School of Electrical Engineering and Computer Science, Washington State University. 9 February 2005. Volume 21, pp 71-82.

[18] Gh. Hamarneh, "Active Shape Models," The Imaging and Image Analysis Group Department of Signals and Systems Chalmers University of Technology Gothenburg, Sweden.

[19] 3D Slicer, http://www.Slicer.org/. Accessed: 20 June, 2015.

[20] Visualization toolkit, http://www.VTK.org/. Accessed: 20 June, 2015.